Acoustic full waveform inversion in time domain using blended data

He. Liu, Daniel. Trad, Kristopher. Innanen

ABSTRACT

Cost is the primary factor that needs to be considered for the seismic data acquisition and processing. Super-shot or blended data strategy has been used in marine and land seismic surveys to reduce acquisition costs by reducing the number of recording times. Full waveform inversion (FWI) has been used to estimate high-resolution subsurface velocity models. However, it suffers from expensive computational cost for matching the synthetic and the observed data. Once the super-shots are acquired, conventional FWI methods would require a de-blending process for super-shots. To reduce the costs of both data acquisition and processing, FWI using blended data without the de-blending stage has been recognized very promising in future oil exploration. In this work, we accelerate the FWI process using different source-encoding strategies and compare their perfomance. The synthetic examples show that amplitude and random time delay encoding provide slow convergence rate and less satisfactory inversion results. The dynamic combined source-encoding strategy converges fast, providing updated velocity with ignorable artifacts. While the static combined source-encoding strategy provides the fast convergence rate as well as good estimation of velocity model. In addition, it requires the minimum computational cost since we can directly simulate the super-shots without the blending stage.

INTRODUCTION

Cost is one of the key factors that affects how a seismic data acquisition will be conducted. Even though the costs of seismic data acquisition and processing have reduced dramatically with significantly improved technology, large seismic surveys are still too expensive for oil industries and raise the demand of data processing at the same time (Beasley et al., 1998).

FWI is a high-resolution seismic imaging technique that is based on using the entire content of seismic traces for extracting physical parameters of the medium sampled by seismic waves (Virieux et al., 2017). The classical time-domain full-waveform inversion (FWI) is originally proposed by Tarantola (1984) to invert the velocity model by minimizing the l2-norm of the difference between predicted and observed data (Symes, 2008). Full-waveform inversion techniques are promising but still suffer from some well-defined obstacles (Pan, 2017), such as the nonlinearity, the non-uniqueness of the solution and the expensive computational cost. The goal of FWI is to match the synthetic and the observed data. The minimization of the misfit function is essentially an iterative, computationally intensive procedure. At each iteration, the gradient of the objective function has to be calculated with respect to the model parameters by cross-correlating the back-propagated residual wavefield with the corresponding forward-propagated source wavefield. The forward modeling demands large computational efforts, whereas back propagation of the residual wavefield has large memory requirements to access the source wavefield. Pica et al. (1990) further applied FWI into elastic cases. Pratt et al. (1998) proposed frequency-domain FWI,

multiscale inversion became an area of active research. To date, building a good velocity model is still a challenging problem and attracts the increasing effort of geophysicists (Virieux and Operto, 2009).

To reduce the costs of both data acquisition and processing, simultaneous source-firing strategy has been recognized very promising in future oil exploration. Increasing field efficiency by recording more than one source has been explored by means of encoded shot gathers or super-shots (Womack et al., 1990; Abma et al., 2015; Anagaw and Sacchi, 2012; Romero et al., 2000; Garottu, 1983) . However, once the super-shots are acquired, traditional seismic processing methods require a de-blending process for velocity model estimation and seismic migration are performed (Florez et al., 2016).

Source-encoding strategies are first introduced into pre-stack migration in frequency domain (Morton and Ober, 1998; Romero et al., 2000), including random phase-encoding, linear phase-encoding, (modified-) chirp phase-encoding strategies, etc. Zhan et al. (2009) proposed to compose multi-source shot gather of a sum of single shot gathers with random time delays. Krebs et al. (2009) proposed to multiply the source wavelet with random encoding sequence of +1 or -1 and then blend all the shot gathers into one super-shot. Dai et al. (2012) proposed to combine these two phase-encoding strategies for least-squares RTM. Hu et al. (2016) proposed an efficient amplitude encoding strategy using cosine basis to perform least-squares reverse time migration. Godwin and Sava (2013) proposed an amplitude encoding strategy using Hartley basis for wave-equation migration and compared it's performance with some other source-encoding strategies. To date, source-encoding strategies have been used to accelerate RTM, LSRTM and FWI process (Krebs et al., 2009; Dai et al., 2012; Godwin and Sava, 2013; Pan, 2017)

In this paper, we compare the inversion results by both random time-delay source-encoding and random polarity source-encoding. We also adopt an amplitude source-encoding method (Hu et al., 2016) into acoustic FWI for comparison. Furthermore, we combined random time-delay and random polarity source-encoding to achieve improved convergence rate and present updated model with well suppressed artifacts.

Acoustic Full Waveform Inversion in Time Domain

In the case of constant density, the acoustic wave equation is described by

$$\frac{1}{v^2(\mathbf{x})}\frac{\partial^2 p\left(\mathbf{x},t;\mathbf{x}_s\right)}{\partial t^2}-\nabla^2 p\left(\mathbf{x},t;\mathbf{x}_s\right)=f_s\left(\mathbf{x},t;\mathbf{x}_s\right) \tag{1}$$

where $f_s\left(x,t;x_s\right)=f\left(t'\right)\delta\left(x-x_s\right)\delta\left(t-t'\right)$.

According to equation 1, the data misfit $\Delta p = p_{cal} - p_{obs}$ can be defined by the differences at the receiver positions between the recorded seismic data p_{obs} and the forward modeled seismic data $p_{\text{cal}} = f(m)$ for each source-receiver pair of the seismic survey. In the acoustic velocity inversion, $f(\cdot)$ indicates the forward modeling function, whereas m corresponds to the velocity model to be inverted. The goal of FWI is to match the data misfit by iteratively updating the velocity model. We also define the data misfit function as the objective function taking the least-squares norm of the misfit vector Δp, which is given

by

$$\begin{aligned} E(\mathbf{m}) &= \frac{1}{2}\Delta\mathbf{p}^{\dagger}\Delta\mathbf{p} = \frac{1}{2}\left\|\mathbf{p}_{\mathrm{cal}}-\mathbf{p}_{\mathrm{obs}}\right\|^{2} \\ &= \frac{1}{2}\sum_{r=1}^{ng}\sum_{s=1}^{ns}\int_{0}^{t_{\max}}\mathrm{d}t\left|p_{\mathrm{cal}}\left(\mathbf{x}_{r},t;\mathbf{x}_{s}\right)-p_{\mathrm{obs}}\left(\mathbf{x}_{r},t;\mathbf{x}_{s}\right)\right|^{2} \end{aligned} \tag{2}$$

where ns and ng are the number of sources and receivers and † denotes the adjoint operator (conjugate transpose).

We use the gradient-based minimization method, which updates the velocity model according to a descent direction $\mathbf{d}_k$ and

$$\mathbf{m}_{k+1} = \mathbf{m}_k + \alpha_k \mathbf{d}_k \tag{3}$$

where k denotes the iteration number. By neglecting higher order terms, the objective function can be approximated by

$$\begin{aligned} E\left(\mathbf{m}_{k+1}\right) &= E\left(\mathbf{m}_k+\alpha_k\mathbf{d}_k\right) \\ &= E\left(\mathbf{m}_k\right)+\alpha_k\left\langle\nabla E\left(\mathbf{m}_k\right),\mathbf{d}_k\right\rangle+\frac{1}{2}\alpha_k^2\mathbf{d}_k^{\dagger}\mathbf{H}_k\mathbf{d}_k \end{aligned} \tag{4}$$

where $\mathbf{H}_k$ stands for the Hessian matrix and $\langle\cdot,\cdot\rangle$ denotes the inner product. Differentiation of the misfit function $E\left(\mathbf{m}_{k+1}\right)$ with respect to α_k gives

$$\alpha_k = -\frac{\left\langle\mathbf{d}_k,\nabla E\left(\mathbf{m}_k\right)\right\rangle}{\mathbf{d}_k^{\dagger}\mathbf{H}_k\mathbf{d}_k} = -\frac{\left\langle\mathbf{d}_k,\nabla E\left(\mathbf{m}_k\right)\right\rangle}{\left\langle\mathbf{J}_k\mathbf{d}_k,\mathbf{J}_k\mathbf{d}_k\right\rangle} = \frac{\left\langle\mathbf{J}_k\mathbf{d}_k,\mathbf{p}_{\mathrm{obs}}-\mathbf{p}_{\mathrm{cal}}\right\rangle}{\left\langle\mathbf{J}_k\mathbf{d}_k,\mathbf{J}_k\mathbf{d}_k\right\rangle} \tag{5}$$

in which we use the approximate Hessian $H_k := H_a = J_k^{\dagger}J_k$ (usually referred to as the approximate Hessian) and $\nabla_m E = J_k^{\dagger}\Delta p$.

The CG algorithm decreases the misfit function along the CG direction, where

$$\mathbf{d}_k = \begin{cases} -\nabla E\left(\mathbf{m}_0\right) & k=0 \\ -\nabla E\left(\mathbf{m}_k\right)+\beta_k\mathbf{d}_{k-1} & k\geq 1 \end{cases} \tag{6}$$

We adopt Yang's (Yang et al., 2015) hybrid scheme combining Hestenes-Stiefel and Dai-Yuan methods to compute β_k (Hager and Zhang, 2006):

$$\beta_k = \max\left(0,\min\left(\beta_k^{\mathrm{HS}},\beta_k^{\mathrm{DY}}\right)\right) \tag{7}$$

where

$$\begin{cases} \beta_k^{\mathrm{HS}} = \frac{\langle\nabla E(\mathbf{m}_k),\nabla E(\mathbf{m}_k)-\nabla E(\mathbf{m}_{k-1})\rangle}{\langle\mathbf{d}_{k-1},\nabla E(\mathbf{m}_k)-\nabla E(\mathbf{m}_{k-1})\rangle} \\ \beta_k^{\mathrm{DY}} = \frac{\langle\nabla E(\mathbf{m}_k),\nabla E(\mathbf{m}_k)\rangle}{\langle\mathbf{d}_{k-1},\nabla E(\mathbf{m}_k)-\nabla E(\mathbf{m}_{k-1})\rangle} \end{cases} \tag{8}$$

The gradient of the misfit function with regards to the model is given by Bunks et al. (1995):

$$\nabla E_{\mathrm{m}} = \frac{2}{v^3(\mathbf{x})}\sum_{r=1}^{ng}\sum_{s=1}^{ns}\int_0^{t_{\max}}\frac{\partial^2 p_{\mathrm{cal}}\left(\mathbf{x},t;\mathbf{x}_s\right)}{\partial t^2}p_{\mathrm{res}}\left(\mathbf{x}_r,t;\mathbf{x}_s\right)\mathrm{d}t \tag{9}$$

where $p_{\text{res}}\left(x_r, t; x_s\right)$ is the back-propagated residual wavefield. A precondition is possible by normalizing the gradient by the source illumination, which is the energy of the forward wavefield accounting for geometric divergence (Bai et al., 2014) :

$$\nabla E\left(\mathrm{m}_k\right) = \frac{\nabla E_{\mathrm{m}}}{\sqrt{\sum_{s=1}^{ns} \int_0^{t_{\max}} p_{\text{cal}}^2\left(x, t; x_s\right) \mathrm{d}t + \gamma^2}} \tag{10}$$

where γ is a stability factor to avoid division by zero. To obtain a reasonable step size α_k in equation 5, we estimate a small step length ε proposed by Pica et al. (1990) :

$$\max\left(\epsilon\left|\mathbf{d}_k\right|\right) \leq \frac{\max\left(\left|\mathbf{m}_k\right|\right)}{100} \tag{11}$$

and the Taylor approximation

$$\mathbf{J}_k \mathbf{d}_k \approx \frac{\mathbf{f}\left(\mathbf{m}_k + \epsilon \mathbf{d}_k\right) - \mathbf{f}\left(\mathbf{m}_k\right)}{\epsilon} \tag{12}$$

For amplitude source-encoding, the encoding matrix is defined as

$$\mathbf{B} = \begin{bmatrix} b^{1,1} & b^{2,1} & . & b^{N_{ig},1} \\ b^{1,2} & b^{2,2} & . & b^{N_{sig},2} \\ . & . & . & . \\ b^{1,N_{sup}} & b^{2,N_{sup}} & . & b^{N_{sig} \cdot N_{sup}} \end{bmatrix} \tag{13}$$

where N_{sup} is the number of the super-shots and N_{sig} is the number of the individual shots. The cosine basis is usually implemented using its discrete form. By selecting the reference distance x_{ref}, the discrete form of the orthogonal cosine basis is (Malvar, 1992)

$$b = \sqrt{\frac{2}{n_{\text{sig}}}} \cos\left(\frac{\pi}{n_{\text{sig}}} \frac{(2iss+1)(2ik+1)}{4}\right) \tag{14}$$

where $iss = j\%n_{sig}, j = 1, 2 \ldots N_{sig}, ik = 1, 2, \ldots N_{sup}$ where $n_{\text{sig}} = x_{\text{ref}}/ds_x$ is the number of the single shots in a reference distance; ds_x is the shot sampling interval; j is the shot index; and ik is the super shot index; $\%$ is the remainder operator.

In this work, we implement FWI process based on Yang's (Yang et al., 2015) program, which incorporates a wavefield reconstruction strategy that only saves the boundaries to accelerate calculation efficiency.

Numerical Results

In this paper, we use a Marmousi model with a distance of 9216 m and a depth of 3008 m on a grid of 16 meters discretized in a grid of 576 by 188 grid points, which is shown in Fig 1a. On top of the Marmousi model is a water layer with the thickness of 320 m, the acoustic velocity is set to 1500 m/s. which makes the whole model size 576 by 208

grid points. We get the initial model shown in Fig 1b by smoothing the original Marmousi model, but the top layer remains not smoothed.

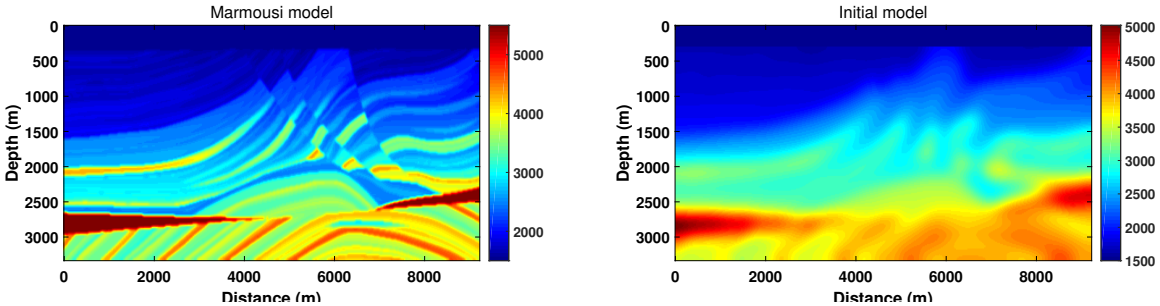

FIG. 1. (a) The original Marmousi is down sampled along depth and lateral direction. The shots are generated according to the Marmousi model. (b) The initial model of FWI for Marmousi model, which is obtained by smoothing the original model.

In this work, we generate all synthetic shot gathers by solving the acoustic wave equations in time domain for all 140 sources, which are evenly distributed near the surface of original Marmousi model with a spatial interval of 64 m (4 grid points). We deploy 576 receivers right beneath the sources with a spatial interval of 16 m (1 grid point). The Ricker wavelet sources are fired with a central frequency of 4 Hz. We record the seismic waveforms for 4.2 s with an time step of 1.5 ms.

For conventional FWI, all the sources are fired individually and shot gathers are recorded separately. For FWI using blended data, multiple sources are fired and blended data are acquired in one seismic survey. Zhan et al. (2009) pointed out that the more shot gathers blended into one super shot, the larger the artifacts or cross-terms generated in the misfit gradient. In this case, instead of blending all the shots into one super-shot, all shots are blended into several sub-super-shots that contain all the shot records (Dai et al., 2012), which would provide better inversion results. The number of super shots is also the factor by which the computational cost is reduced. In our experiments, we compare the updated velocity obtained by FWI using different source-encoding strategies with 10 blended super-shots, which are linear combinations of the individual shot gathers.

In the first case, we use amplitude encoding method to generate blended data. For this method, it usually assigns different weights to all the individual shot gathers and blend them into one super-shot. In our experiment, we choose the reference distance as a quater of the model distance, which makes the N_{sig} 35. The amplitude encoding matrix is shown in Fig 2. Using the time-delay source-encoding strategy, all the sources are excited with random time delay with the maximum delay value of 0.6 s. We blend every 14 shot-gathers into 1 super-shot, so we obtain 10 super-shots over all. In the third case, we simulate all the 140 shot gathers in a conventional way and multiply them with random polarity encoding sequence of +1 or -1 at every iteration, then we also blend them into 10 super-shots in the same way. For Krebs's source-encoding strategy, changing the encoding between iterations produces artifacts that do not add coherently and are therefore better suppressed (Krebs et al., 2009).

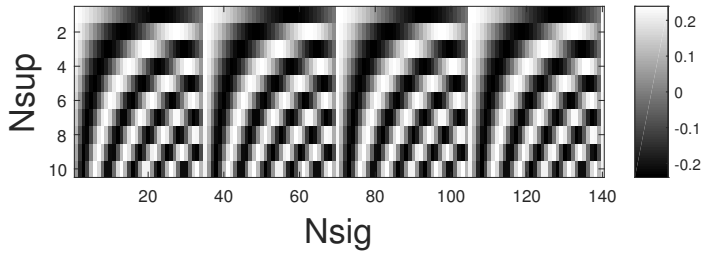

FIG. 2. The amplitude source-encoding matrix.

In this work, we also combine the random time delay and random polarity source-encoding strategies to perform acoustic FWI. So the encoding functions are the combination of source-side random time delay and random source polarities. We experiment two cases: static encoding and dynamic encoding. Static encoding keeps the encoding function to be the same at all the iterations, while a purely dynamic strategy changes the encoding function at each iteration (Krebs et al., 2009; Dai et al., 2012). In this way, using this combined source-encoding strategy, we can get the super-shots encoded with both random time delay and random polarity. In the first case, we multiply the shot gathers with random time delay with random encoding sequence of +1 or -1 and blend them into 10 super-shots. In the second case, we change the random polarity encoding sequence and regenerate the blended data at every iteration.

For the same Marmousi model, we simulate the blended data using different source-encoding strategies and carry out FWI process for 150 iterations to compare the inversion results. Fig 3 gives the first super-shot in different cases. All the individual shot gathers are encoded into one super-shot using amplitude encoding (see Fig 3a), while other super-shots contain only 14 shot gathers (see Fig 3b, c and d). Fig 3d is first super-shot using static encoding and dynamic encoding at the first iteration.

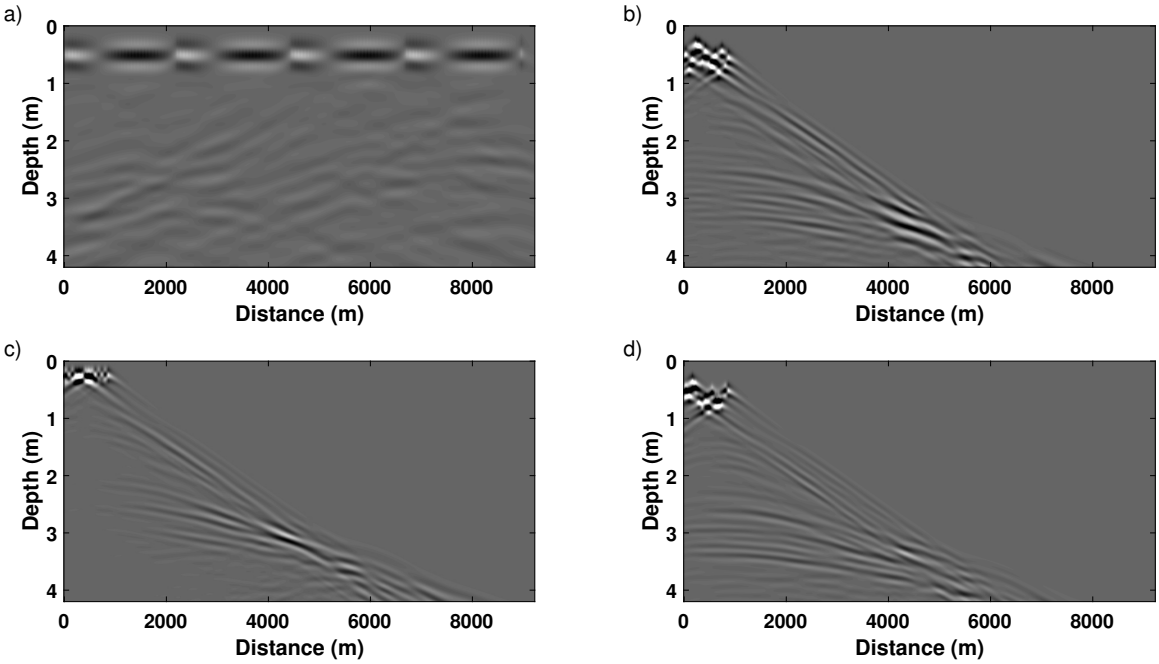

FIG. 3. Synthetic first super-shot for acoustic FWI using blended data: (a) the first super-shot encoded with amplitude matrix; (b) the first super-shot encoded with random time delay; (c) the first super-shot encoded with random polarity; (d) the first super-shot encoded with both of random time delay and random polarity.

We also record all the updated models for all the strategies at all the iterations. The updated velocity models at iteration 10, 50 and 150 are displayed in Fig 4, Fig 5 and Fig 6. FWI using blended data usually would result in noise, which is caused by the crosstalk between the encoded sources, and it is much stronger in early iterations, see Fig 4 and Fig 5 (Krebs et al., 2009).

From the comparison of updated velocity models, we can notice that the amplitude encoding and the random time delay encoding strategy provide the most unsatisfactory results (see Fig 6a and Fig 6b). With increasing iteration times, they would still introduce increasingly obvious cross talk noise (see Fig 5a and b), which results from the interference between the encoded sources. In addition, they show slower convergence rate.

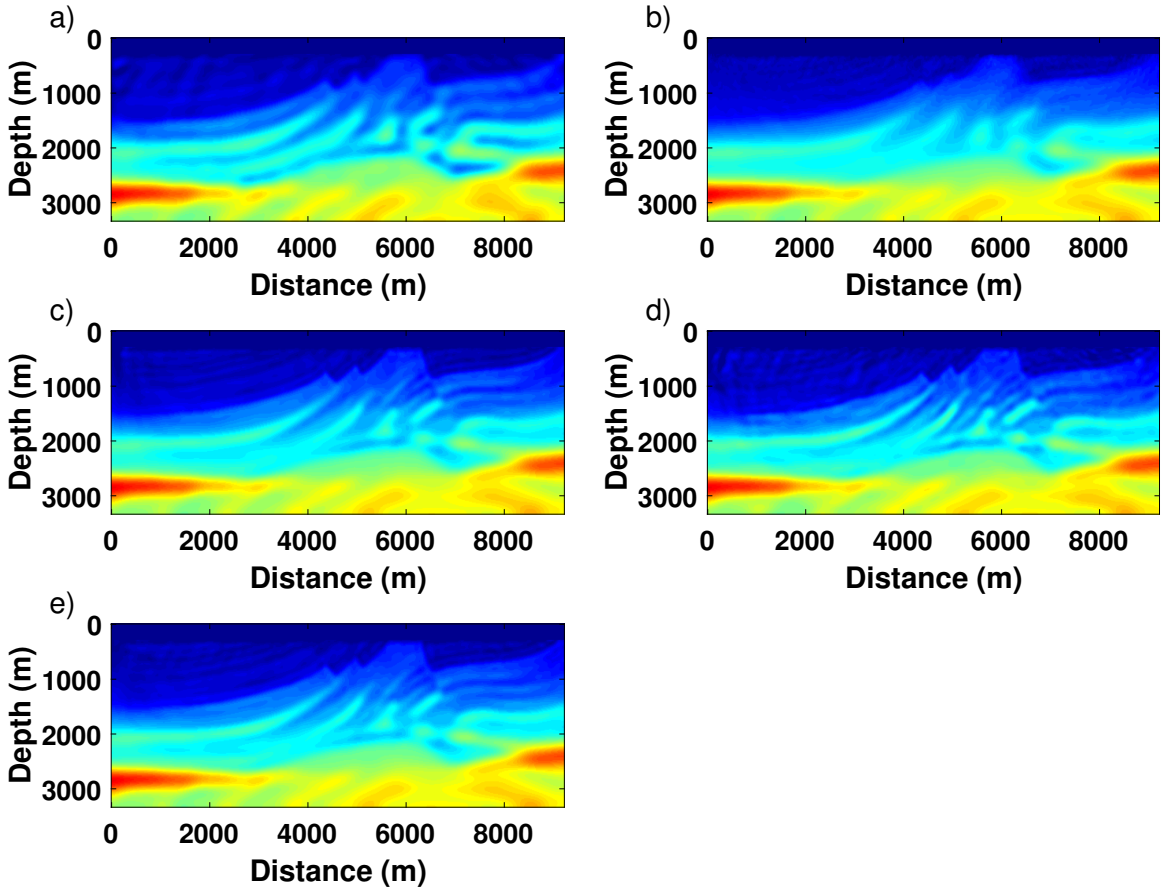

FIG. 4. Inversion results after 10 iterations: (a) amplitude encoding; (b) random time delay; (c) random polarity; (d) static encoding; (e) dynamic encoding.

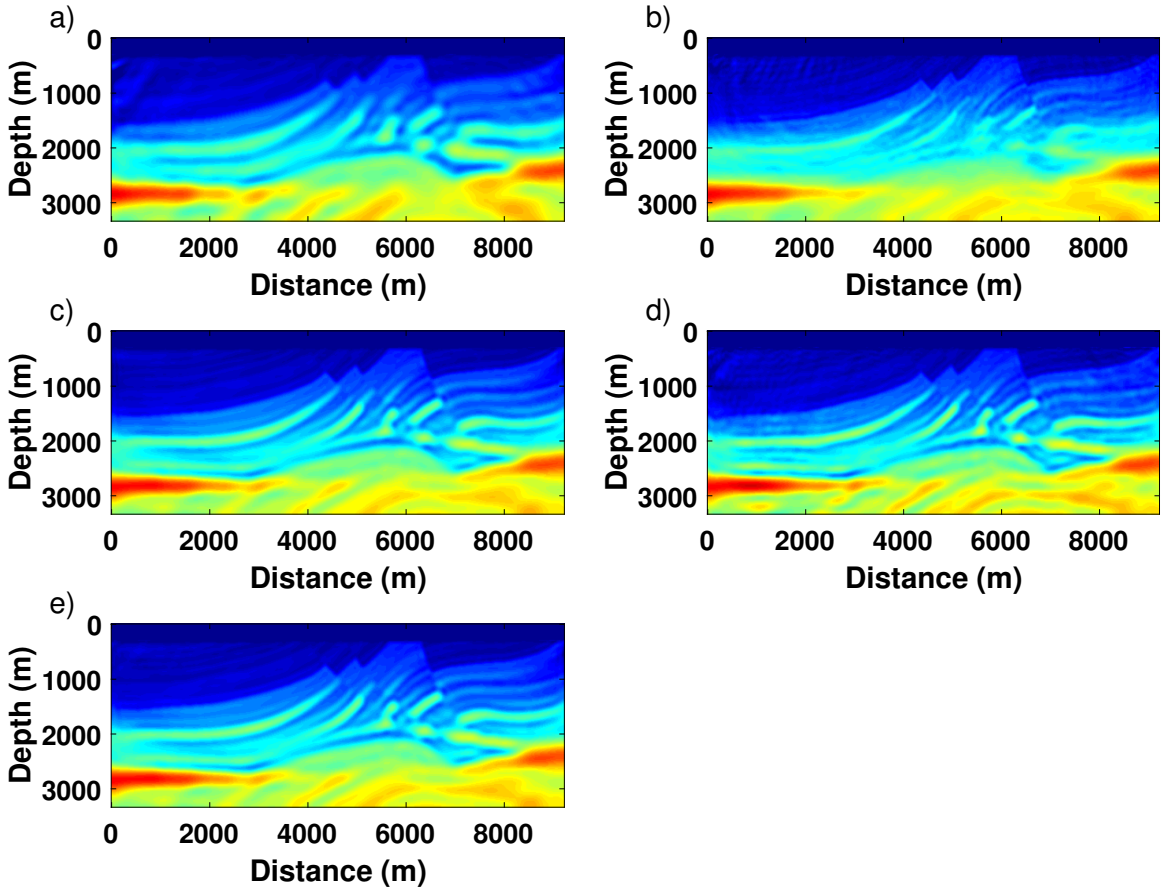

FIG. 5. Inversion results after 50 iterations: (a) amplitude encoding; (b) random time delay; (c) random polarity; (d) static encoding; (e) dynamic encoding.

From Fig 6c and Fig 6e, we can notice that whenever the random polarity is used to generate the super-shots and the encoding sequences are changed at each iteration, they provide very similar results with ignorable artifacts which are very close to the original Marmousi model.

We can also notice that, when we apply the static encoding strategy without changing the encoding sequences, whose results are shown in Fig 4d, Fig 5d and Fig 6d. With increasing iteration times, the artifacts would increase at first and then decrease as the iteration continues to increase, which means even when we don't change the encoding sequence in our experiment, this combined source-encoding strategy could also suppress the cross talk well. What's more important is that, compared to the updated velocity models, this static encoding strategy provides the updated velocity model very close to the original model with very fast convergence, describing better big and very fine high velocity structures at large depth. And this is different from the other cases even though there are still some minor artifacts at the left of the velocity model, which would not significantly affect geologic interpretation of the inverted image. We present the vertical profiles at two different locations in Fig 7.

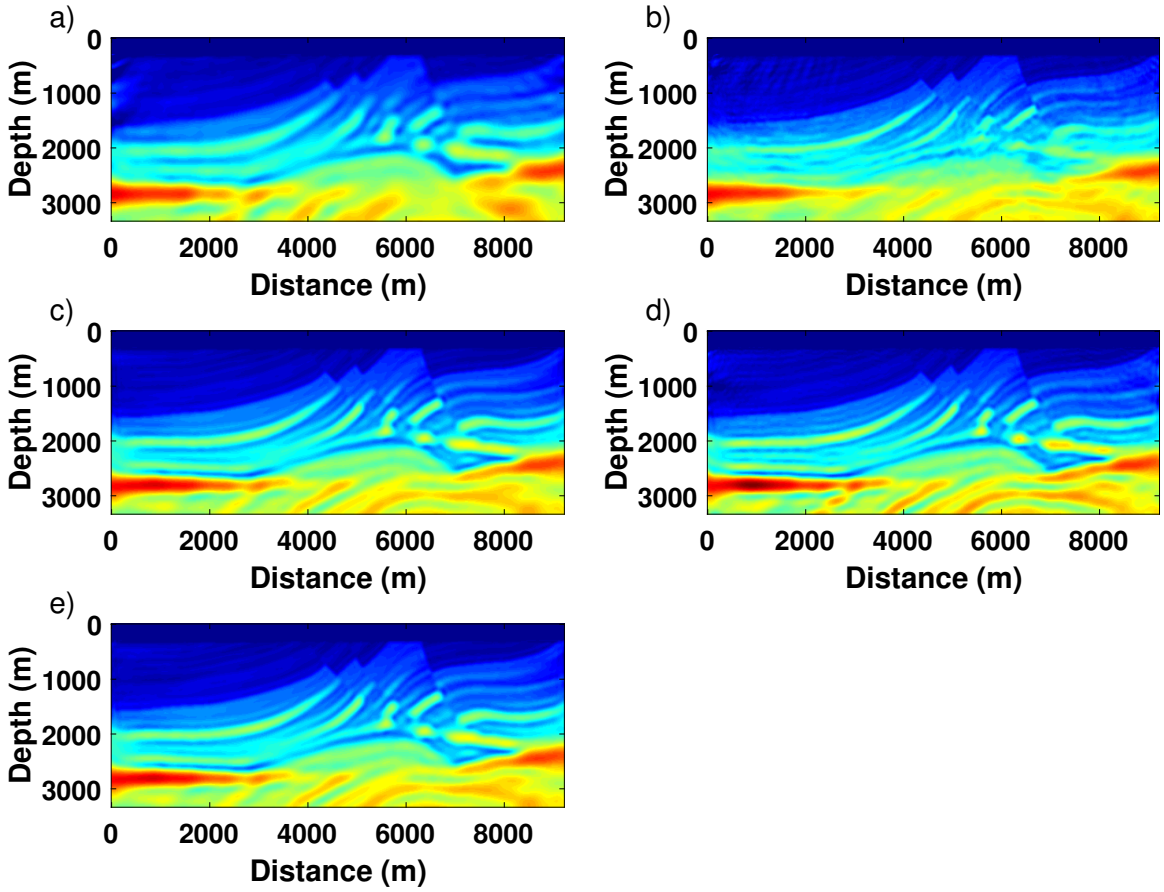

FIG. 6. Inversion results after 150 iterations: (a) amplitude encoding; (b) random time delay; (c) random polarity; (d) static encoding; (e) dynamic encoding.

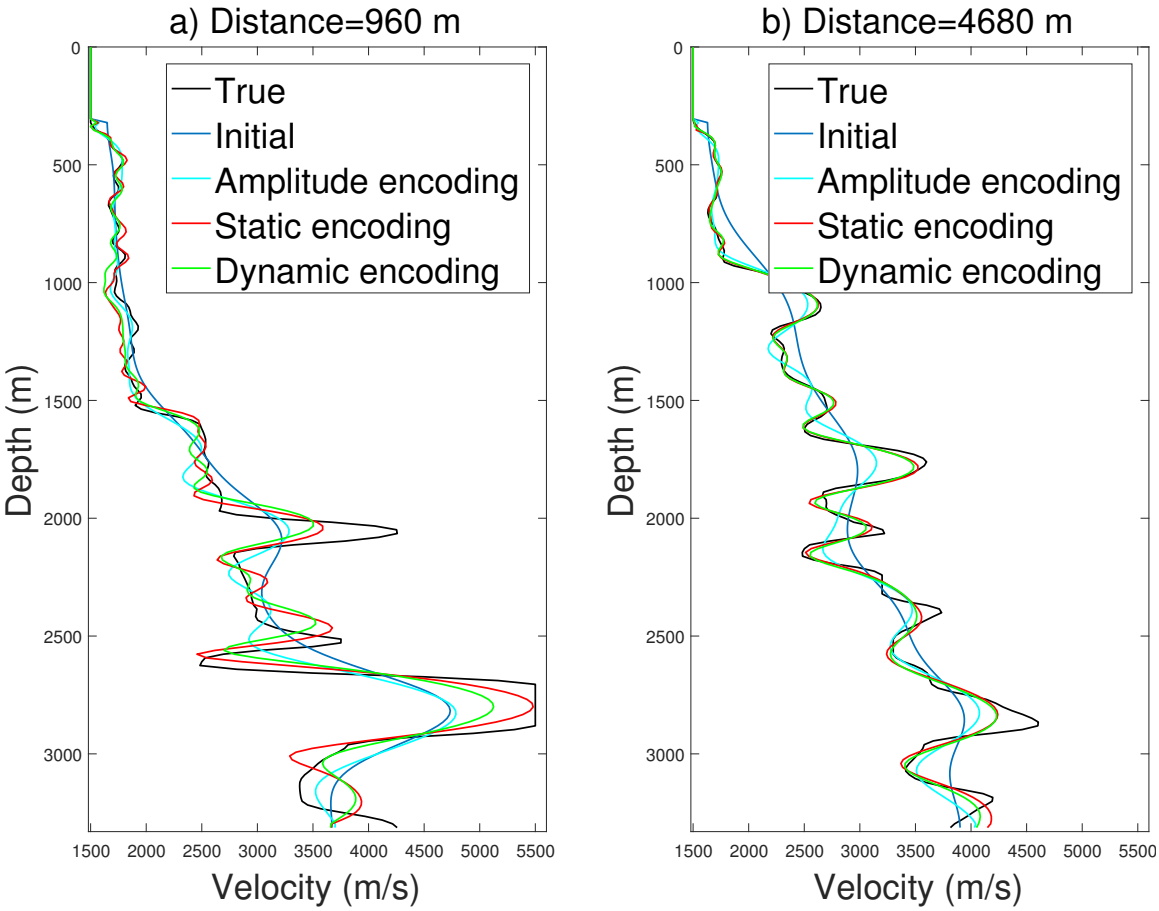

FIG. 7. Comparison of vertical profiles between the true, initial and inverted velocity models using amplitude, static and dynamic encoding at different locations.

To further compare the performance of these algorithms and investigate the convergence rate, we compare the model misfit (l2-norm of the difference between updated velocity model and original Marmousi model) versus iteration, which is displayed in Fig 8. From the comparison, we can notice that the amplitude encoding and the random time delay strategy provide slow convergence rate (see Fig 8) as well as less satisfactory updated velocity models (see Fig 6a and Fig 6b). As the iteration continues, the model misfit decrease very slow. As for the random polarity and dynamic encoding, they show very similar convergence rate, which is also verified by the inversion results shown in Fig 6. Consistent with inversion results, the convergence rate curve of FWI using static encoding stays underneath other curves of other cases.

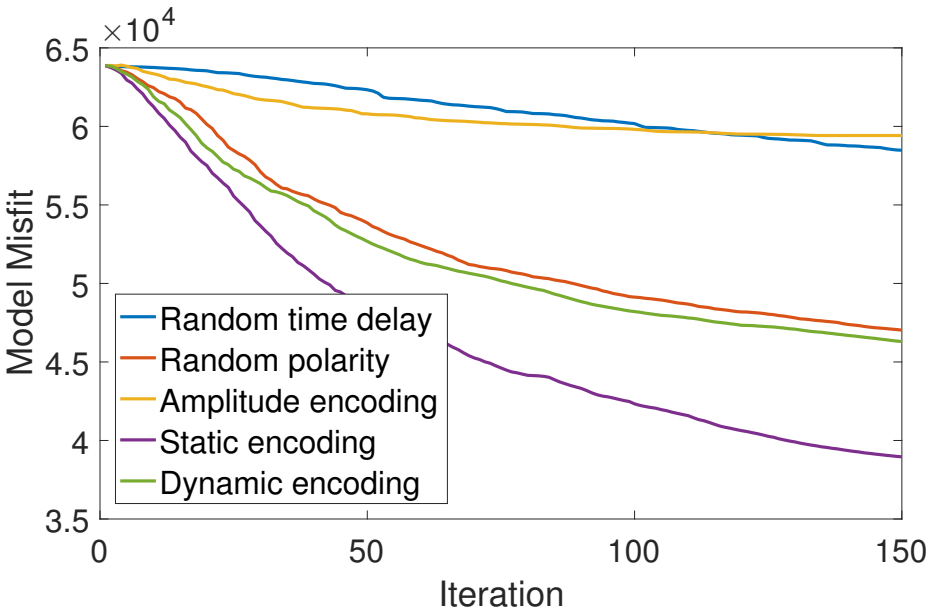

FIG. 8. Comparison of model misfit versus iteration for FWI using different source-encoding strategies: random time delay, random polarity, amplitude encoding, static encoding and dynamic encoding.

CONCLUSIONS

FWI using blended data can avoid the de-blending stage and reduces both of field data acquisition and computational cost of forward modelling process times in FWI procedure. In this paper, we presented the acoustic FWI results using different source-encoding strategies and compared their performance.

In our experiments, for conventional FWI, it requires 140 times of forward modelling to generate the synthetic acoustic data. While for FWI using random time delay and static source encoding, we can directly simulate 10 super-shots without the blending stage to improve the calculation efficiency for both forward modelling and FWI inversion process. For amplitude, random polarity and dynamic encoding strategies, they still require 140 times of solving acoustic wave equations and then generate blended data, which will directly increase the calculation cost. As for the dynamic encoding, it even requires generating the blended data using a different sequence at each iteration, which will further increase the I/O cost.

Through the synthetic examples, we can notice that the static combined source-encoding strategy which uses both of random time delay and random polarity as the encoding function provides the fastest convergence rate and satisfactory updated velocity model, even though there still remains minor artifacts. For FWI using the dynamic combined source-encoding strategy, it also converges fast and provides updated velocity model with ignorable artifacts. However, considering the calculation efficiency, it requires extra computational cost of forward modelling and I/O cost with a factor directly associated with the number of blended data and iteration times.

ACKNOWLEDGMENTS

We thank the sponsors of CREWES for continued support. This work was funded by CREWES industrial sponsors, NSERC (Natural Science and Engineering Research Council of Canada) through the grants CRDPJ 461179-13 and CRDPJ 543578-19. Partial funding also came from the Canada First Research Excellence Fund.

The implementation of acoustic FWI in time domain used in this study is adopted from Pengliang Yang's work. We thank Pengliang Yang for his codes contributed to the Madagascar.

REFERENCES

Abma, R., Howe, D., Foster, M., Ahmed, I., Tanis, M., Zhang, Q., Arogunmati, A., and Alexander, G., 2015, Independent simultaneous source acquisition and processing: Geophysics, **80**, No. 6, WD37–WD44.

Anagaw, A., and Sacchi, M., 2012, Full waveform inversion using blended acquisition geometry with different frequency strategies, *in* 74th EAGE Conference and Exhibition incorporating EUROPEC 2012, European Association of Geoscientists & Engineers, cp–293.

Bai, J., Yingst, D., Bloor, R., and Leveille, J., 2014, Viscoacoustic waveform inversion of velocity structures in the time domainviscoacoustic waveform inversion: Geophysics, **79**, No. 3, R103–R119.

Beasley, C., Chambers, R., and Jiang, Z., 1998, A new look at simultaneous sources: Seg technical program expanded abstracts.

Bunks, C., Saleck, F. M., Zaleski, S., and Chavent, G., 1995, Multiscale seismic waveform inversion: Geophysics, **60**, No. 5, 1457–1473.

Dai, W., Fowler, P., and Schuster, G. T., 2012, Multi-source least-squares reverse time migration: Geophysical Prospecting, **60**, No. 4-Simultaneous Source Methods for Seismic Data, 681–695.

Florez, K. A., Mantilla, J. G., and Ramirez, A. B., 2016, Full waveform inversion (fwi) in time for seismic data acquired using a blended geometry, *in* 2016 XXI Symposium on Signal Processing, Images and Artificial Vision (STSIVA), IEEE, 1–5.

Garottu, R., 1983, Simultaneous recording of several vibroseis® seismic lines, *in* SEG Technical Program Expanded Abstracts 1983, Society of Exploration Geophysicists, 308–310.

Godwin, J., and Sava, P., 2013, A comparison of shot-encoding schemes for wave-equation migration: Geophysical Prospecting, **61**, 391–408.

Hager, W. W., and Zhang, H., 2006, A survey of nonlinear conjugate gradient methods: Pacific journal of Optimization, **2**, No. 1, 35–58.

Hu, J., Wang, H., Fang, Z., Li, T., and Zhang, J., 2016, Efficient amplitude encoding least-squares reverse time migration using cosine basis: Geophysical prospecting, **64**, No. 6, 1483–1497.

Krebs, J. R., Anderson, J. E., Hinkley, D., Neelamani, R., Lee, S., Baumstein, A., and Lacasse, M.-D., 2009, Fast full-wavefield seismic inversion using encoded sources: Geophysics, **74**, No. 6, WCC177–WCC188.

Malvar, H., 1992, Signal processing with lapped transforms. boston: Artech house.

Morton, S. A., and Ober, C. C., 1998, Fastershot-record depth migrations using phase encoding, *in* SEG Technical Program Expanded Abstracts 1998, Society of Exploration Geophysicists, 1131–1134.

Pan, W., 2017, Waveform inversion for estimating subsurface properties: phase-encoding strategies, optimization methods, interparameter tradeoffs quantification and reduction.

Pica, A., Diet, J., and Tarantola, A., 1990, Nonlinear inversion of seismic reflection data in a laterally invariant medium: Geophysics, **55**, No. 3, 284–292.

Pratt, R. G., Shin, C., and Hick, G., 1998, Gauss–newton and full newton methods in frequency–space seismic waveform inversion: Geophysical Journal International, **133**, No. 2, 341–362.

Romero, L. A., Ghiglia, D. C., Ober, C. C., and Morton, S. A., 2000, Phase encoding of shot records in prestack migration: Geophysics, **65**, No. 2, 426–436.

Symes, W. W., 2008, Migration velocity analysis and waveform inversion: Geophysical prospecting, **56**, No. 6, 765–790.

Tarantola, A., 1984, Inversion of seismic reflection data in the acoustic approximation: Geophysics, **49**, No. 8, 1259–1266.

Virieux, J., Asnaashari, A., Brossier, R., Métivier, L., Ribodetti, A., and Zhou, W., 2017, An introduction to full waveform inversion, *in* Encyclopedia of exploration geophysics, Society of Exploration Geophysicists, R1–1.

Virieux, J., and Operto, S., 2009, An overview of full-waveform inversion in exploration geophysics: Geophysics, **74**, No. 6, WCC1–WCC26.

Womack, J., Cruz, J., Rigdon, H., and Hoover, G., 1990, Encoding techniques for multiple source point seismic data acquisition: Geophysics, **55**, No. 10, 1389–1396.

Yang, P., Gao, J., and Wang, B., 2014, Rtm using effective boundary saving: A staggered grid gpu implementation: Computers & Geosciences, **68**, 64–72.

Yang, P., Gao, J., and Wang, B., 2015, A graphics processing unit implementation of time-domain full-waveform inversion: Geophysics, **80**, No. 3, F31–F39.

Zhan, G., Boonyasiriwat, C., Dai, W., and Schuster, G., 2009, Multi-source waveform inversion with deblurring: Journal of seismic exploration.